JAM CM Journal of Applied Mathematics and Computational Mechanics 2024, 23(2), 41-53
www.amcm.pcz.pl p-ISSN 2299-9965
DOI: 10.17512/jamcm.2024.2.04 e-ISSN 2353-0588

NUMERICAL MODELING OF TISSUE LASER IRRADIATION WITH UNCERTAIN PARAMETERS USING THE INTERVAL FINITE POINTSET METHOD

Anna Korczak

Department of Computational Mechanics and Engineering, Silesian University of Technology
Gliwice, Poland
anna.korczak@polsl.pl

Received: 8 November 2023; Accepted: 13 March 2024

Abstract. In the following paper, the numerical analysis of thermal processes occurring in biological tissue with uncertain parameters is presented. The heat transfer model is based on the Pennes equation, where interval heat sources are introduced. The model is assumed to be transient and one-dimensional. Additionally, analysed tissue is exposed to laser irradiation, and the internal heat sources resulting from laser irradiation based on the Beer law are taken into account. Moreover, the perfusion rate and the effective scattering coefficient are treated as variables dependent on tissue damage. For numerical calculations, the interval version of the Finite Pointset Method has been used. All calculations are performed due to the direct interval arithmetic rules. The paper is concluded by presenting the obtained results.

MSC 2010: *65M99, 80A20*
Keywords: *Finite Pointset Method, meshless methods, bioheat transfer, interval arithmetic*

1. Introduction

In this study, the application of the Finite Pointset Method (FPM) to solve heat transfer problem in biological tissue with uncertain parameters introduced as directed interval numbers is presented. The heat transfer model is based on the Pennes equation, considering the model as transient and one-dimensional [1, 2]. Moreover, the paper considers the impact of laser irradiation, which is represented through a model based on the Beer law. This law describes the attenuation of laser energy as it passes through tissue. Understanding this aspect is essential for gaining a comprehensive insight into the absorption and conversion of laser energy into thermal energy within the tissue [3]. This knowledge is extremely important across a range of sectors, particularly in medical domains like laser therapy, in oncology, and surgical techniques. The integration of laser technology in medical practices has seen substantial growth, underscoring the need to grasp the fundamental mechanisms and enhance their effectiveness.

It is assumed that the perfusion rate and the effective scattering coefficient in the model depend on tissue injury. This accounts for the ever-changing nature of tissue response to laser irradiation, where alterations in blood flow and tissue properties can arise due to thermal damage [4].

In the computational part of this study, the interval version of the FPM has been applied, to the best of the author's knowledge, for the first time. Directed interval arithmetic as a way of introducing uncertainties of parameters has already been successfully applied in other topics like the solution of the Boltzmann transfer equation [5], modelling of heat transfer during cryopreservation [6], or the analysis of the tissue damage during the heating process [7].

The classical version of the FPM adopts a Lagrangian approach that is fully meshless [8]. The FPM relies on the weighted least-squares technique to estimate spatial derivatives and solve elliptic partial differential equations. It has already been applied in various fields, including fluid mechanics [9, 10], radiative and conductive heat transfer problems [11], and linear elasticity-related issues [12]. Notably, one of the key advantages of this meshless approach is its capacity to handle complex geometries and irregular boundaries [13]. In problems with the fast changes in the computational domain of the fluid, like Fluid-Structure-Interactions, the FPM found its application as well [14]. In contrast to the conventional Finite Element Method or Finite Difference Method, the FPM does not necessitate a structured mesh. Instead, it employs a collection of scattered nodes throughout the domain, making it exceptionally versatile for intricate geometrical configurations.

2. The Pennes equation with interval parameters

The Pennes bioheat partial differential equation, along with its suitable boundary conditions, serves as a mathematical framework employed for depicting the temperature distribution within biological tissues when exposed to diverse heat sources, such as laser irradiation. This equation considers parameters like heat conduction, volumetric specific heat, perfusion (blood flow), metabolic heat production, and the ab-sorption of heat from external sources. Especially values of heat sources are difficult to estimate, as indicated by the various mathematical models used to describe them. For this reason, it was decided in this article to especially treat these parameters (among others) as uncertain and define them as directed interval functions:

$$\overline{Q}(x,t) = \overline{Q}_{perf}(x,t) + \overline{Q}_{met} + \overline{Q}_{las}(x,t) \tag{1}$$

where $\overline{Q}_{perf}, \overline{Q}_{met}, \overline{Q}_{las}$ [W/m^3] are the interval heat sources connected with perfusion, metabolism and laser irradiation.

The basic form of the Pennes equation in the 1D domain with direct interval parameters is as follows [4]:

$$c\frac{\partial \overline{T}}{\partial t}(x,t)=\lambda\frac{\partial^2 \overline{T}}{\partial x^2}(x,t)+\overline{Q}(x,t) \tag{2}$$

where λ [W/(m K)] is the thermal conductivity, c [J/(m^3 K)] is the volumetric specific heat. Moreover, $\overline{T}$ [°C] is the interval temperature, t [s] is the time, and x [m] denotes the spatial coordinate.

The considered interval laser heat source is defined based on the Beer's law and introducing direct interval parameters [15]:

$$\overline{Q}_{las}(x,t)=\overline{\mu}_t'\overline{I}_0\exp\left(-\overline{\mu}_t'x\right)s(t) \tag{3}$$

where $\overline{I}_0$ [W m^{-2}] is the interval surface irradiance of the laser and $s(t)$ is the function equal to 1 when the laser is on and equal to 0 when the laser is off, whereas $\overline{\mu}_t'$ [m^{-1}] is the interval attenuation coefficient defined as:

$$\overline{\mu}_t'=\overline{\mu}_a+\overline{\mu}_s' \tag{4}$$

where $\overline{\mu}_a$ [m^{-1}] is the interval absorption coefficient and $\overline{\mu}_s'$ [m^{-1}] is the interval effective scattering coefficient that can be treated as a constant value or as a function of the interval injury Arrhenius integral as well:

$$\overline{\mu}_s'\left(\overline{\theta}\right)=\overline{\mu}_{snat}'\exp\left(-\overline{\theta}\right)+\overline{\mu}_{sden}'\left(1-\exp\left(-\overline{\theta}\right)\right) \tag{5}$$

The interval injury Arrhenius integral is defined as [4]:

$$\overline{\theta}(x,t)=\int_0^t A\exp\left[-\frac{\Delta E}{R\overline{T}\left(x,\hat{t}\right)}\right]d\hat{t} \tag{6}$$

where A [s^{-1}] is the pre-exponential factor, ΔE [J mole^{-1}] is the activation energy of the reaction R [J mole^{-1} K^{-1}] is a universal gas constant (for values of parameters see Table 3).

The interval perfusion heat source function is taken into account is as follows:

$$\overline{Q}_{perf}(x,t)=c_B\overline{G}_B(x,t)\left(T_B-\overline{T}(x,t)\right) \tag{7}$$

where $\overline{G}_B$ [(m$^3_{\text{blood}}$ s^{-1})/(m$^3_{\text{tissue}}$)] is the interval blood perfusion rate, c_B [J m^{-3} K^{-1}] is the volumetric specific heat of blood while T_B [°C] denotes the artery temperature. Additionally, the interval blood perfusion coefficient is a function determined based on the tissue's necrotic alterations [4]:

$$\overline{G}_B\left(\overline{\theta}(x,t)\right)=\overline{G}_{B0}\overline{w}\left(\overline{\theta}(x,t)\right) \tag{8}$$

where $\overline{G}_{B0}$ represents the interval initial perfusion rate, and we assume that function w follows an interval polynomial form [4]:

$$\overline{w}\left(\theta\left(x,t\right)\right)=\sum_{j=1}^{3}m_j\theta\left(x,t\right)^{j-1} \tag{9}$$

where m_j are specified coefficients (see Table 2).

Moreover, equation (1) must be supplemented by the boundary-initial conditions. The analysed model is supplemented by the boundary condition of the third type on a tissue surface subjected to a laser irradiation

$$x=0:\ -\lambda\frac{\partial\overline{T}}{\partial n_0}=\alpha\left(\overline{T}\left(x,t\right)-T_{amb}\right) \tag{10}$$

where n_0 [m] is an external normal vector ($n_0=[n_x, n_y, n_z]$), α [W m^{-2} K^{-1}] is the convective heat transfer coefficient and T_{amb} [°C] is the temperature of the surrounding area. On the internal tissue surface ($x = L$), the adiabatic condition is assumed. The initial distribution of temperature has been assumed as a constant value T_0 [°C].

The suggested interval model more accurately represents the heat transfer process in living tissue when compared to the classical Pennes equation, which assumes single-valued thermal and optical parameters. The interval Pennes equation must be solved numerically due to the rules of the interval arithmetic to predict the temperature distribution in a form of intervals. In this paper, it is proposed to apply the interval FPM which is described in detail in Section 3.

3. The Interval Finite Pointset Method

The FPM is a meshless Lagrangian approach that employs the weighted least-squares interpolation technique to estimate spatial derivatives and solve partial differential equations [9]. The FPM uses Taylor series to calculate function and derivative values, which naturally emerge as unknown coefficients in the series. A more comprehensive guide on applying the classical version of the FPM can be found in various literature sources [8-12]. In this section, we will outline the fundamental concept of the interval version of the FPM (called further Interval Finite Pointset Method), specifically applied to the Pennes equation. This method (IFPM) is a result of applying directed interval arithmetic to the FPM. The parameters considered as directed interval numbers are described in detail in Section 2.

First, the main idea of the classical version of the FPM needs to be explained. For this purpose let's consider a domain X with a defined boundary. The description included here is intentionally for three dimensional space, although numerical examples are presented for a one dimensional case. Within this domain X, we have a collection of n points $x_1, x_2, \ldots, x_n$ ($x_j=[x_j^1, x_j^2, x_j^3]$, $j = 1, \ldots, n$), each associated

with respective function values $f(x_1), f(x_2), \ldots, f(x_n)$. The objective is to approximate the value of f at an arbitrary location x ($x = [x^1, x^2, x^3]$). To achieve this, we define the approximation of $f(x_j)$ using a Taylor series expansion ($dx_j^k = x_j^k - x^k$, $k = 1, 2, 3$) centered around x:

$$\tilde{f}\left(x_j\right) = f\left(x\right) + \sum_{k=1}^{3} f_k\left(x\right) dx_j^k + \frac{1}{2} \sum_{k,l=1}^{3} f_{kl}\left(x\right) dx_j^k dx_j^l \tag{11}$$

The values that are not known $f(x)$, $f_k(x)$, $f_{kl}(x)$, ($k = 1, 2, 3$, $l = 1, 2, 3$) are obtained from a weighted least squares method achieved by minimizing the quadratic expression while considering all neighbor points (*np*):

$$J = \sum_{j=1}^{np} w_j \left(Ma - b\right)^2 \tag{12}$$

where $w_j = w\left(x_j, x\right)$ and

$$w\left(x_j, x\right) = \begin{cases} \exp\left(-\beta \left\| x_j - x \right\|^2 / h^2\right), & \left\| x_j - x \right\| \le h \\ 0, \text{ otherwise} \end{cases} \tag{13}$$

where β is a positive constant. The value h is a radius that defines a set of neighbor points around x.
Equation (12) can be expressed in the form:

$$J = \left(Ma - b\right)^T W \left(Ma - b\right) \tag{14}$$

where

$$W = \begin{pmatrix} w\left(x_1, x\right) & 0 & \cdots & 0 \\ 0 & w\left(x_2, x\right) & 0 & 0 \\ \vdots & \vdots & \ddots & \vdots \\ 0 & 0 & \cdots & w\left(x_{np}, x\right) \end{pmatrix} \tag{15}$$

Formally, the minimization of the function J results in:

$$a = \left(M^T W M\right)^{-1} \left(M^T W\right) b \tag{16}$$

In this point, we assume that x belongs to the interior part of X. Moreover matrix M, taking into account equation (11) for all neighbor points around x, then adding

the Pennes equation (here the unknown function is denoted f and Δt is a time step) that must be satisfied (2), is defined as follows:

$$M = \begin{pmatrix} 1 & dx_1^1 & dx_1^2 & dx_1^3 & \frac{1}{2}\left(dx_1^1\right)^2 & dx_1^1 dx_1^2 & dx_1^1 dx_1^3 & \frac{1}{2}\left(dx_1^2\right)^2 & dx_1^2 dx_1^3 & \frac{1}{2}\left(dx_1^3\right)^2 \\ 1 & dx_2^1 & dx_2^2 & dx_2^3 & \frac{1}{2}\left(dx_2^1\right)^2 & dx_2^1 dx_2^2 & dx_2^1 dx_2^3 & \frac{1}{2}\left(dx_2^2\right)^2 & dx_2^2 dx_2^3 & \frac{1}{2}\left(dx_2^3\right)^2 \\ \vdots & \vdots & \vdots & \vdots & \vdots & \vdots & \vdots & \vdots & \vdots & \vdots \\ 1 & dx_{np}^1 & dx_{np}^2 & dx_{np}^3 & \frac{1}{2}\left(dx_{np}^1\right)^2 & dx_{np}^1 dx_{np}^2 & dx_{np}^1 dx_{np}^3 & \frac{1}{2}\left(dx_{np}^2\right)^2 & dx_{np}^2 dx_{np}^3 & \frac{1}{2}\left(dx_{np}^3\right)^2 \\ 2c & 0 & 0 & 0 & -\lambda\Delta t & 0 & 0 & -\lambda\Delta t & 0 & -\lambda\Delta t \end{pmatrix} \tag{17}$$

Then a and b take the following form (τ is a time counter):

$$a = \left[f(x), f_1(x), f_2(x), f_3(x), f_{12}(x), f_{13}(x), f_{22}(x), f_{23}(x), f_{33}(x) \right]^T \tag{18}$$

$$b = \left[f^{\tau+1}(x_1), f^{\tau+1}(x_2), \ldots, f^{\tau+1}(x_{np}), 2\Delta t Q^\tau + 2cf^\tau(x) + \lambda\Delta t \nabla^2 f^\tau(x) \right]^T \tag{19}$$

Now, introducing interval parameters (see Section 2), equation (16) takes the following form

$$\overline{a} = \left(M^T W M\right)^{-1} \left(M^T W\right) \overline{b} \tag{20}$$

where unknown interval vector $\overline{a}$ and vector $\overline{b}$ (from now unknown function f is treated as temperature and denoted $\overline{T}$ (as a particular case) are defined as

$$\begin{aligned} \overline{a} = \big[& \overline{T}(x,t), \overline{T}_1(x,t), \overline{T}_2(x,t), \overline{T}_3(x,t), \overline{T}_{12}(x,t), \overline{T}_{13}(x,t), \\ & \overline{T}_{22}(x,t), \overline{T}_{23}(x,t), \overline{T}_{33}(x,t) \big]^T \end{aligned} \tag{21}$$

and

$$\overline{b} = \left[\overline{T}^{\tau+1}(x_1,t), \overline{T}^{\tau+1}(x_2,t), \ldots, \overline{T}^{\tau+1}(x_{np},t), 2\Delta t \overline{Q}^\tau + 2c\overline{T}^\tau(x,t) + \lambda\Delta t \nabla^2 \overline{T}^\tau(x,t) \right]^T \tag{22}$$

Furthermore, the IFPM operates as an iterative technique where vector $\overline{a}$ due to the formula (20) is recalculating over each particle. The implemented algorithm

employs a stopping criterion based on a relative error applied to the upper and the lower bound of temperature intervals $\left(\overline{T}=\left[T^{-},T^{+}\right]\right)$ that have the following structure:

$$\begin{cases} \dfrac{\sum_{j=1}^{np}\left|\left(T^{l+1,\tau}\left(x_j,t\right)\right)^{-}-\left(T^{l,\tau}\left(x_j,t\right)\right)^{-}\right|}{\sum_{j=1}^{np}\left|\left(T^{l+1,\tau}\left(x_j,t\right)\right)^{-}\right|}<\varepsilon \\ \dfrac{\sum_{j=1}^{np}\left|\left(T^{l+1,\tau}\left(x_j,t\right)\right)^{+}-\left(T^{l,\tau}\left(x_j,t\right)\right)^{+}\right|}{\sum_{j=1}^{np}\left|\left(T^{l+1,\tau}\left(x_j,t\right)\right)^{+}\right|}<\varepsilon \end{cases} \tag{23}$$

where l is iteration counter, ε is the maximum relative error.

It is worth mentioning that if point x belongs to the edge of X and satisfies the second of the third type of boundary condition, one extra row must be added in matrix (17) and one extra element in vector (19), because we have one equation more. For the Neumann boundary condition $\left(-\lambda\dfrac{\partial\overline{T}}{\partial n}=\overline{q}_b\right)$, where the adiabatic condition is its particular case for $\overline{q}_b=\left[0,0\right]$, we have:

$$M=\begin{pmatrix} 1 & dx_1^1 & dx_1^2 & dx_1^3 & \frac{1}{2}\left(dx_1^1\right)^2 & dx_1^1dx_1^2 & dx_1^1dx_1^3 & \frac{1}{2}\left(dx_1^2\right)^2 & dx_1^2dx_1^3 & \frac{1}{2}\left(dx_1^3\right)^2 \\ 1 & dx_2^1 & dx_2^2 & dx_2^3 & \frac{1}{2}\left(dx_2^1\right)^2 & dx_2^1dx_2^2 & dx_2^1dx_2^3 & \frac{1}{2}\left(dx_2^2\right)^2 & dx_2^2dx_2^3 & \frac{1}{2}\left(dx_2^3\right)^2 \\ \vdots & \vdots & \vdots & \vdots & \vdots & \vdots & \vdots & \vdots & \vdots & \vdots \\ 1 & dx_{np}^1 & dx_{np}^2 & dx_{np}^3 & \frac{1}{2}\left(dx_{np}^1\right)^2 & dx_{np}^1dx_{np}^2 & dx_{np}^1dx_{np}^3 & \frac{1}{2}\left(dx_{np}^2\right)^2 & dx_{np}^2dx_{np}^3 & \frac{1}{2}\left(dx_{np}^3\right)^2 \\ 2c & 0 & 0 & 0 & -\lambda\Delta t & 0 & 0 & -\lambda\Delta t & 0 & -\lambda\Delta t \\ 0 & \lambda n_x & \lambda n_y & \lambda n_z & 0 & 0 & 0 & 0 & 0 & 0 \end{pmatrix} \tag{24}$$

$$\overline{b}=\left[\overline{T}^{\tau+1}\left(x_1,t\right),\overline{T}^{\tau+1}\left(x_2,t\right),\ldots,\overline{T}^{\tau+1}\left(x_{np},t\right),\right.$$
$$\left.2\Delta t\overline{Q}^{\tau}+2c\overline{T}^{\tau}\left(x,t\right)+\lambda\Delta t\nabla^2\overline{T}^{\tau}\left(x,t\right),-\overline{q}_b\right]^T \tag{25}$$

And then for the Robin boundary condition (see Eq. (10)), we have:

$$M = \begin{pmatrix} 1 & dx_1^1 & dx_1^2 & dx_1^3 & \frac{1}{2}\left(dx_1^1\right)^2 & dx_1^1 dx_1^2 & dx_1^1 dx_1^3 & \frac{1}{2}\left(dx_1^2\right)^2 & dx_1^2 dx_1^3 & \frac{1}{2}\left(dx_1^3\right)^2 \\ 1 & dx_2^1 & dx_2^2 & dx_2^3 & \frac{1}{2}\left(dx_2^1\right)^2 & dx_2^1 dx_2^2 & dx_2^1 dx_2^3 & \frac{1}{2}\left(dx_2^2\right)^2 & dx_2^2 dx_2^3 & \frac{1}{2}\left(dx_2^3\right)^2 \\ \vdots & \vdots & \vdots & \vdots & \vdots & \vdots & \vdots & \vdots & \vdots & \vdots \\ 1 & dx_{np}^1 & dx_{np}^2 & dx_{np}^3 & \frac{1}{2}\left(dx_{np}^1\right)^2 & dx_{np}^1 dx_{np}^2 & dx_{np}^1 dx_{np}^3 & \frac{1}{2}\left(dx_{np}^2\right)^2 & dx_{np}^2 dx_{np}^3 & \frac{1}{2}\left(dx_{np}^3\right)^2 \\ 2c & 0 & 0 & 0 & -\lambda\Delta t & 0 & 0 & -\lambda\Delta t & 0 & -\lambda\Delta t \\ \alpha & \lambda n_x & \lambda n_y & \lambda n_z & 0 & 0 & 0 & 0 & 0 & 0 \end{pmatrix} \tag{26}$$

$$\bar{b} = \Big[\bar{T}^{\tau+1}\left(x_1,t\right), \bar{T}^{\tau+1}\left(x_2,t\right), \ldots, \bar{T}^{\tau+1}\left(x_{np},t\right), 2\Delta t\bar{Q}^{\tau} + 2c\bar{T}^{\tau}\left(x,t\right) + \lambda\Delta t\nabla^2\bar{T}^{\tau}\left(x,t\right), \alpha T_{amb}\Big]^T \tag{27}$$

4. Numerical examples

The study concludes by presenting the obtained results of numerical calculations. These results are not only essential for advancing our understanding of thermal processes in biological tissues, but they also have practical implications in the field of laser applications. By comparing interval results (see Fig. 1) with single-valued ones, the research contributes to the ongoing evaluation and refinement of the proposed computational technic. The single-valued results are always in the range of the temperature intervals as they are presented.

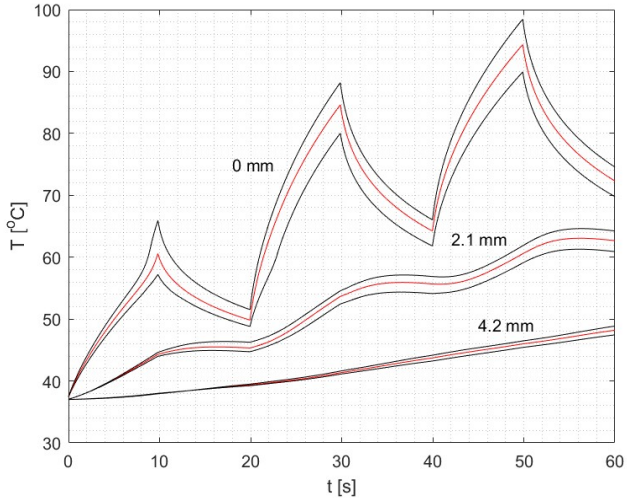

Fig. 1. Courses of temperature intervals (black line) in three different points of the domain for $x = 0$, 2.1, 4.2 mm for $u = 5$ % comparing to the single-valued results (red line)

In this example of numerical computations, the simulation of interval laser irradiation was analysed. Irradiation consisted of consecutive heating and cooling periods that last 10 seconds each. The single-valued thermo-optical parameters of tissue that have been assumed are gathered in Table 1, whereas Arrhenius injury integral parameters in Table 2 and the coefficients appearing in the w function (8) in Table 2. In the tissue region, of the depth of $L = 35$ mm, described in detail in [16], the distribution of points is considered as a regular structure and has been generated with the step $\Delta x = 0.35$ mm, time step Δt is set to 0.1 s, radius that determine neighbour points in the FPM $h = 2.5\Delta x$ and parameter $\beta = 7$ in (13).

Table 1. Thermo-optical parameters [16]

Symbol	Parameter	Value	Unit
λ	Thermal conductivity of tissue	0.609	W m^{-1} K^{-1}
c	Volumetric specific heat of tissue	4.18	MJ m^{-3} K^{-1}
G_{B0}	Initial blood perfusion coefficient	0.00125	s^{-1}
μ_a	Absorption coefficient of tissue	40	m^{-1}
$\mu'_{s\,nat}$	Effective scattering coefficient of native tissue	1000	m^{-1}
$\mu'_{s\,den}$	Effective scattering coefficient of destructed tissue	4000	m^{-1}
Q_{met}	Metabolic heat source	245	W m^{-3}
c_B	Volumetric specific heat of blood	3.9962	MJ m^{-3} K^{-1}
T_B	Arterial blood temperature	37	°C

Table 2. The coefficients of the perfusion coefficient function [4]

	m_1	m_2	m_3
$\theta = 0$	1	0	0
$0 < \theta \le 0.1$	1	25	–260
$0.1 < \theta \le 1$	1	–1	0
$\theta > 1$	0	0	0

Table 3. Arrhenius injury integral parameters [16]

Symbol	Parameter	Value	Unit
A	Pre-exponential factor	$3.1 \cdot 10^{98}$	s^{-1}
ΔE	Activation energy	$6.27 \cdot 10^{5}$	J mole^{-1}
R	Universal gas constant	8.314	J mole^{-1} K^{-1}

The analysed model is supplemented by the boundary condition of the third type on tissue surface subjected to laser irradiation, while on the internal tissue surface the adiabatic condition is assumed. For the boundary condition of the third type, the following input data have been introduced: $\alpha = 8\ \mathrm{W\,m^{-2}\,K^{-1}}$ (the convective heat transfer coefficient) and $T_{amb} = 20\ ^\circ\mathrm{C}$ (the temperature of surrounding). The initial distribution of temperature has been assumed as a constant value $T_0 = 37\ ^\circ\mathrm{C}$. The peak power laser intensity is considered as $I_0 = 30\ \mathrm{kW\,m^{-2}}$. Calculations were performed in three different points of the depth 0, 2.1, 4.2 mm with the stopping criterion (23) for $\varepsilon = 10^{-4}$. Input parameters like: initial blood perfusion coefficient, absorption coefficient of tissue, effective scattering coefficient of native tissue, effective scattering coefficient of destructed tissue, metabolic heat source and peak power intensity were treated as directed intervals.

Those parameters of tissue, which were assumed as the directed interval numbers, are in the following form

$$\overline{p} = \left[p^{-}, p^{+} \right] = \left[p - p \cdot u\%, p + p \cdot u\% \right] \tag{28}$$

where p denotes parameter and u defines the width of the interval [7].
In the calculations, u is assumed to be 2.5 % or 5 %. Results for both values are compared in Figure 2. As it can be observed, temperature intervals are wider for wider intervals of the input parameters.

Moreover, calculations for other interval parameters like the injury integral, the laser heat source and the effective scattering coefficient were done (Figs. 3-5).

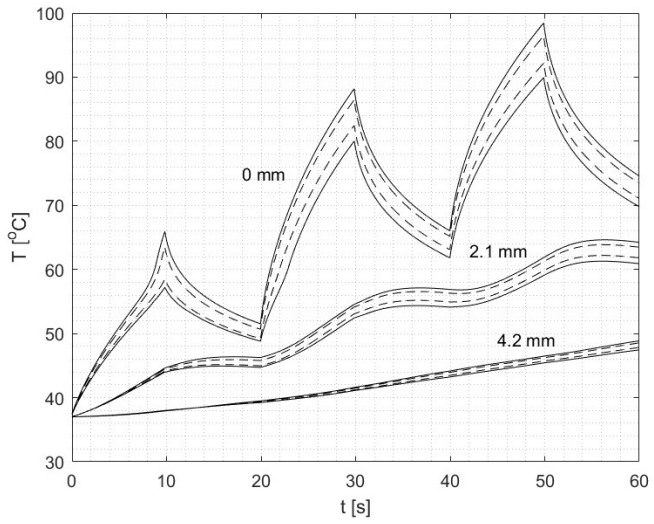

Fig. 2. Courses of temperature intervals in three different points of the domain for $x = 0$, 2.1, 4.2 mm for $u = 2.5$ % (dashed line) and $u = 5$ % (solid line)

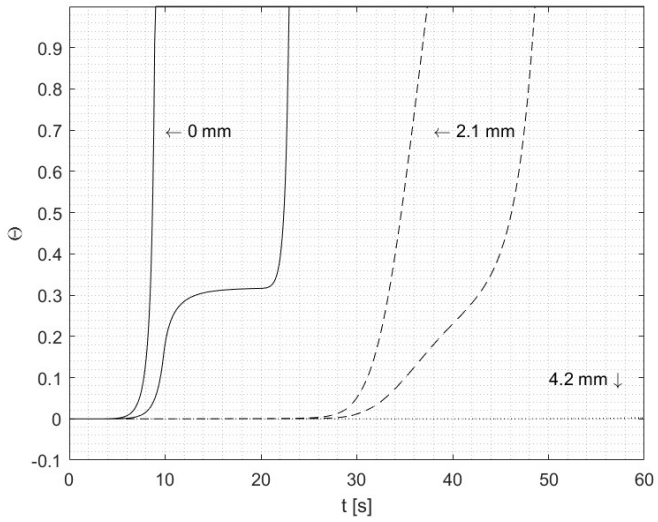

Fig. 3. Courses of the interval injury integral in three different points of the domain for $x = 0$, 2.1, 4.2 mm for $u = 5$ %

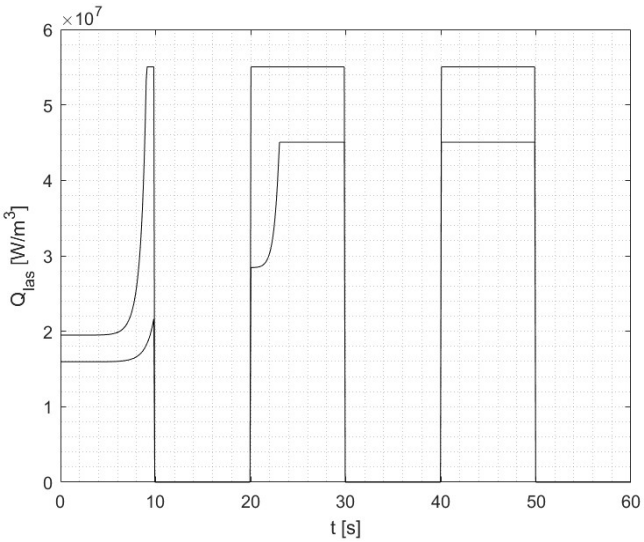

Fig. 4. Course of the interval laser heat source in three different points of the domain for $x = 0$, 2.1, 4.2 mm for $u = 5$ %

By analysing the graph with courses of interval temperatures for two different values of u (Fig. 2), we can observe that in three pick points for $x = 0$, which can be important from a practical point of view, were obtained following interval temperatures (in °C): [58.5, 62.9], [82.5, 86.5], [96.2, 92.2] for $u = 2.5\%$ and [56.9, 65.5], [79.8, 88.2], [89.9, 98.3] for $u = 5\%$. This gives a temperature range of widths successively: 4.4, 4, 4 °C and 8.6, 8.4, 8.4 °C.

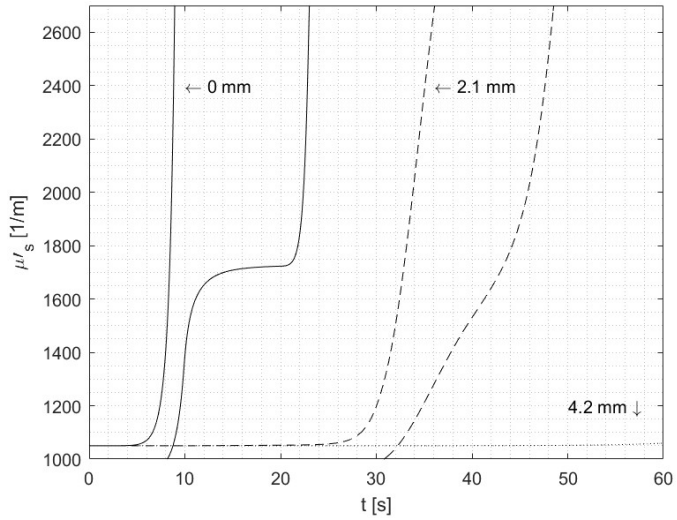

Fig. 5. Courses of the interval effective scattering coefficient in three different points of the domain for x = 0, 2.1, 4.2 mm for u = 5 %

From Figure 3 (u = 5 %) can be observed when the injury integral achieves value 1, which means complete tissue necrosis, and it is between 9 and 22 seconds. The same time moments can be observed in Figure 5, when the effective scattering coefficient started to be a constant value.

5. Conclusions

This paper explores how the IFPM can be effectively applied to the transient bioheat transfer problems with uncertain parameters. Analysed numerical method is appropriate for solving complex problems related to temperature and necrosis dependent parameters. This makes it a good option for modeling the dynamic thermal processes within biological tissue when subjected to laser irradiation, particularly when dealing with more intricate mathematical models. Another benefit of this approach is its straightforward application of boundary conditions, which opens up the potential for using it in scenarios involving multi-layered domains or 3D problems. The validity of the IFPM method was performed, as could be observed in Figure 1, where comparison with the classical FPM is presented.

Acknowledgments

The research is funded from projects of the Silesian University of Technology, Faculty of Mechanical Engineering.

References

[1] Gupta, P.K., Singh, J., Rai, K.N., & Rai, S.K. (2013). Solution of the heat transfer problem in tissues during hyperthermia by finite difference-decomposition method. *Applied Mathematics and Computation*, *219*(12), 6882-6892.

[2] Karaa, S., Zhang, J., & Yang, F. (2005). A numerical study of a 3D bioheat transfer problem with different spatial heating. *Mathematics and Computers in Simulation*, *68*(4), 375-388.

[3] Jasiński, M. (2015). Modelling of thermal damage in laser irradiated tissue. *Journal of Applied Mathematics and Computational Mechanics*, *14*(4), 67-78.

[4] Abraham, J.P., & Sparrow, E.M. (2007). A thermal-ablation bioheat model including liquid-to--vapor phase change, pressure- and necrosis-dependent perfusion, and moisture-dependent properties. *International Journal of Heat and Mass Transfer*, *50*(13-14), 2537-2544.

[5] Paruch, M., Piasecka-Belkhayat, A., & Korczak, A. (2023). Identification of the ultra-short laser parameters during irradiation of thin metal films using the interval lattice Boltzmann method and evolutionary algorithm. *Advances in Engineering Software*, *180*, 103456.

[6] Skorupa, A., & Piasecka-Belkhayat, A. (2023). Comparison of heat transfer phenomena for two different cryopreservation methods: slow freezing and vitrification. *Journal of Applied Mathematics and Computational Mechanics*, *22*(1), 53-65.

[7] Korczak, A., & Jasiński, M. (2019). Modelling of biological tissue damage process with application of interval arithmetic. *Journal of Theoretical and Applied Mechanics*, *57*(1), 249-261.

[8] Kuhnert, J. (1999). *General Smoothed Particle Hydrodynamics, Ph.D. thesis*. Technische Universität Kaiserslautern.

[9] Tiwari, S., & Kuhnert, J. (2001). Grid free method for solving the Poisson equation. *Berichte Des Fraunhofer ITWM*, *25*.

[10] Saucedo-Zendejo, F.R., & Nóbrega, J.M. (2022). A novel approach to model the flow of generalized Newtonian fluids with the finite pointset method. *Computational Particle Mechanics*, *9*(4), 585-595.

[11] Wawreńczuk, A., Kuhnert, J., & Siedow, N. (2007). FPM computations of glass cooling with radiation. *Computer Methods in Applied Mechanics and Engineering*, *196*(45-48), 4656-4671.

[12] Saucedo-Zendejo, F.R., & Reséndiz-Flores, E.O. (2020). Meshfree numerical approach based on the Finite Pointset Method for static linear elasticity problems. *Computer Methods in Applied Mechanics and Engineering*, *372*, 113367.

[13] Reséndiz-Flores, E.O., & Saucedo-Zendejo, F.R. (2018). Numerical simulation of coupled fluid flow and heat transfer with phase change using the Finite Pointset Method. *International Journal of Thermal Sciences*, *133*, 13-21.

[14] Uhlmann, E., Barth, E., Seifarth, T., Höchel, M., Kuhnert, J., & Eisenträger, A. (2020). Simulation of metal cutting with cutting fluid using the Finite-Pointset-Method. *Procedia CIRP*, *101*, 98-101.

[15] Glenn, T.N., Rastegar, S., & Jacques, S.L. (1996). Finite element analysis of temperature controlled coagulation in laser irradiated tissue. *IEEE Transactions on Biomedical Engineering*, *43*(1), 79.

[16] Jasiński, M. (2010). Numerical modeling of tissue coagulation during laser irradiation controlled by surface temperature. *Scientific Research of the Institute of Mathematics and Computer Science*, *9*(1), 29-36.